Research Article | Vol. 25, No. 25 | 11 Dec 2017 | OPTICS EXPRESS 31045
Optics EXPRESS

Analysis and magnetic modulation of chiro-optical properties in anisotropic chiral and magneto-chiral plasmonic systems

HUA YU FENG, CAROLINA DE DIOS, FERNANDO GARCÍA, ALFONSO CEBOLLADA, AND GASPAR ARMELLES*

IMN-Instituto de Micro y Nanotecnología de Madrid (CNM-CSIC), Isaac Newton 8, PTM, Tres Cantos, E-28760 Madrid, Spain
**gaspar@imm.cnm.csic.es*

Abstract: We present a systematic study to separate the different contributions to the dichroic response of complex plasmonic split-ring/ring magneto-chiral systems. For this, we first construct metastructures with plasmonic, chiral and magneto-optical functionalities by specific arrangements of different building blocks, each of them responsible for one of the functionalities. Then, by the use of Mueller matrices in forward/backward spectroscopic measurements under magnetic field, we separate optical anisotropy from pure chiral contributions to the overall dichroic response of the system. This allows determining the pure chiral response of the structures and the corresponding magnetic field modulation mediated by the magneto-optical effect present in the corresponding building block, which reaches values of 25% at 740 nm. This fabrication and characterization procedure, assigning the different optical functionalities to different building blocks, and decomposing the different contributions to the global optical response, allows an easy and rational identification of the different phenomena exhibited by the magneto-chiral system.

OCIS codes: (260.2130) Ellipsometry and polarimetry; (250.5403) Plasmonics; (230.3810) Magneto-optic systems; (160.1585) Chiral media.

References and links

1. L. A. Nguyen, H. He, and C. Pham-Huy, "Chiral drugs: an overview," Int. J. Biomed. Sci. **2**(2), 85–100 (2006).
2. Y. Tang and A. E. Cohen, "Optical chirality and its interaction with matter," Phys. Rev. Lett. **104**(16), 163901 (2010).
3. A. Guerrero-Martínez, J. L. Alonso-Gómez, B. Auguié, M. M. Cid, and L. M. Liz-Marzán, "From individual to collective chirality in metal nanoparticles," Nano Today **6**, 381–400 (2011).
4. V. K. Valev, J. J. Baumberg, C. Sibilia, and T. Verbiest, "Chirality and chiroptical effects in plasmonic nanostructures: fundamentals, recent progress, and outlook," Adv. Mater. **25**(18), 2517–2534 (2013).
5. A. Ben-Moshe, B. M. Maoz, A. O. Govorov, and G. Markovich, "Chirality and chiroptical effects in inorganic nanocrystal systems with plasmon and exciton resonances," Chem. Soc. Rev. **42**(16), 7028–7041 (2013).
6. M. Hentschel, M. Schäferling, X. Duan, H. Giessen, and N. Liu, "Chiral plasmonics," Sci. Adv. **3**(5), e1602735 (2017).
7. E. Hendry, T. Carpy, J. Johnston, M. Popland, R. V. Mikhaylovskiy, A. J. Lapthorn, S. M. Kelly, L. D. Barron, N. Gadegaard, and M. Kadodwala, "Ultrasensitive detection and characterization of biomolecules using superchiral fields," Nat. Nanotechnol. **5**(11), 783–787 (2010).
8. Y. Zhao, A. N. Askarpour, L. Sun, J. Shi, X. Li, and A. Alù, "Chirality detection of enantiomers using twisted optical metamaterials," Nat. Commun. **8**, 14180 (2017).
9. G. Armelles, B. Caballero, P. Prieto, F. García, A. Cebollada, M. U. González, and A. García-Martin, "Magnetic field modulation of chirooptical effects in magnetoplasmonic structures," Nanoscale **6**(7), 3737–3741 (2014).
10. G. Armelles, A. Cebollada, H. Y. Feng, A. García-Martín, D. Meneses-Rodríguez, J. Zhao, and H. Giessen, "Interaction effects between magnetic and chiral building blocks: a new route for tunable magneto-chiral plasmonic structures," ACS Photonics **2**, 1272–1277 (2015).
11. H. Fujiwara, *Spectroscopic Ellipsometry. Principles and Applications* (John Wiley & Sons, 2007).
12. O. Arteaga, "Number of independent parameters in the Mueller matrix representation of homogeneous depolarizing media," Opt. Lett. **38**(7), 1131–1133 (2013).
13. H. Y. Feng, F. Luo, R. Arenal, L. Henrard, F. García, G. Armelles, and A. Cebollada, "Active magnetoplasmonic split-ring/ring nanoantennas," Nanoscale **9**(1), 37–44 (2017).

#309055 https://doi.org/10.1364/OE.25.031045
Journal © 2017 Received 13 Oct 2017; revised 15 Nov 2017; accepted 16 Nov 2017; published 28 Nov 2017

Optics EXPRESS

14. P. Yu, S. Chen, J. Li, H. Cheng, Z. Li, and J. Tian, "Co-enhancing and -confining the electric and magnetic fields of the broken-nanoring and the composite nanoring by azimuthally polarized excitation," Opt. Express **21**(18), 20611–20619 (2013).
15. S. Cataldo, J. Zhao, F. Neubrech, B. Frank, C. Zhang, P. V. Braun, and H. Giessen, "Hole-mask colloidal nanolithography for large-area low-cost metamaterials and antenna-assisted surface-enhanced infrared absorption substrates," ACS Nano **6**(1), 979–985 (2012).
16. J. Zhao, B. Frank, F. Neubrech, C. Zhang, P. V. Braun, and H. Giessen, "Hole-mask colloidal nanolithography combined with tilted-angle-rotation evaporation: A versatile method for fabrication of low-cost and large-area complex plasmonic nanostructures and metamaterials," Beilstein J. Nanotechnol. **5**, 577–586 (2014).
17. R. Ogier, Y. Fang, M. Svedendahl, P. Johansson, and M. Käll, "Macroscopic layers of chiral plasmonic nanoparticle oligomers from colloidal lithography," ACS Photonics **1**, 1074–1081 (2014).
18. H. Fredriksson, Y. Alaverdyan, A. Dmitriev, C. Langhammer, D. S. Sutherland, M. Zäch, and B. Kasemo, "Hole-mask colloidal lithography," Adv. Mater. **19**, 4297–4302 (2007).
19. M. H. Wiedmann, M. H. Engel, R. A. Van Leeuwen, K. Mibu, T. Shinjo, and C. M. Falco, "Anomalous perpendicular anisotropy in thin Co films," Proc. MRS **313**, 531–536 (1993).
20. D. Kuiper, W. Hoving, A. P. van de Mosselaer, and W. Howing; F.J. den Broeder; A.P. van de Mosselaer, "Perpendicular magnetic anisotropy of Co-Au multilayers induced by interface sharpening," Phys. Rev. Lett. **60**(26), 2769–2772 (1988).
21. B. D. H. Tellegen, "The gyrator, a new electric network element," Philips Res. Rep. **3**, 81–101 (1948).
22. O. Arteaga, "Spectroscopic sensing of reflection optical activity in achiral $AgGaS_2$," Opt. Lett. **40**(18), 4277–4280 (2015).
23. N. Berova, L. Di Bari, and G. Pescitelli, "Application of electronic circular dichroism in configurational and conformational analysis of organic compounds," Chem. Soc. Rev. **36**(6), 914–931 (2007).
24. A. Guerrero-Martínez, B. Auguié, J. L. Alonso-Gómez, Z. Dzolic, S. Gómez-Graña, M. M. Mladen Zinic, M.M. Cid, and L. M. Liz-Marzán, "Intense optical activity from three-dimensional chiral ordering of plasmonic nanoantennas," Angew. Chem. Int. Ed. **50**, 5499–5503 (2011).
25. B. Yeom, H. Zhang, H. Zhang, J. I. Park, K. Kim, A. O. Govorov, and N. A. Kotov, "Chiral plasmonic nanostructures on achiral nanopillars," Nano Lett. **13**(11), 5277–5283 (2013).
26. X. Lan, X. Lu, C. Shen, Y. Ke, W. Ni, and Q. Wang, "Au nanorod helical superstructures with designed chirality," J. Am. Chem. Soc. **137**(1), 457–462 (2015).
27. D. Meneses-Rodríguez, E. Ferreiro-Vila, P. Prieto, J. Anguita, M. U. González, J. M. García-Martín, A. Cebollada, A. García-Martín, and G. Armelles, "Probing the electromagnetic field distribution within a metallic nanodisk," Small **7**(23), 3317–3323 (2011).
28. V. Yannopapas and A. Vanakaras, "Strong magnetochiral dichroism in suspensions of magnetoplasmonic nanohelices," ACS Photonics **2**, 1030–1038 (2015).
29. V. Yannopapas, "Magnetochirality in hierarchical magnetoplasmonic clusters," Solid State Commun. **217**, 47 (2015).
30. G. L. J. A. Rikken and E. Raupach, "Observation of magneto-chiral dichroism," Nature **390**, 493–494 (1997).
31. S. Eslami, J. G. Gibbs, Y. Rechkemmer, J. van Slageren, M. Alarcón-Correa, T.-C. Lee, A. G. Mark, G. L. J. A. Rikken, and P. Fisher, "Chiral nanomagnets," ACS Photonics **1**, 1231–1236 (2014).

1. Introduction

Natural or artificial chiral substances interact differently with circularly polarized light, the intensity (dichroism) or phase (birefringence) of the light transmitted through them depending on the relative handedness of the substance and the light. This fact can be applied to the detection or quantification of a specific enantiomer (left or right chiral counterpart) of a substance in a sample. If the nature of this substance is such that one of its enantiomers can involve for example health issues if ingested, the quest for routes for specific enantiomer differentiation and quantification is of obvious interest [1]. In this sense, the design, fabrication and study of plasmonic structures with some kind of chiral configuration has recently attracted a lot of attention, since they open the route to generate intense electromagnetic fields of suitable symmetries to enhance light-chiral matter interaction [2-6]. This fact immediately translates into the possibility to improve the current detection limits of chiral substances by the use of this approach [7,8].

Seeking for strategies to further improve the sensitivity of these resonant chiral metasystems, a possibility consists of introducing some kind of functionality that allows modulating the chiral light-matter interaction, so that an active, rather than passive, detection platform can be developed. One route to endorse this active character is to incorporate a ferromagnetic component into the equation, making it possible to modulate the chiral response of the resulting system with an external magnetic field thanks to the magneto-optical

Optics EXPRESS

(MO) activity of the ferromagnet [9, 10]. However, a fact that must not be disregarded is that now the total dichroic response of such a system will be due to the contribution, not only of the intrinsic (say, configurational) chirality, but also of the MO nature of the active element (magnetic circular dichroism, MCD), and even from the eventual presence of optical anisotropies which may also give rise to circular dichroism (CD). Therefore, in order to clarify the origin of the differences in absorption between left and right circularly polarized light, one has to develop a measurement protocol that allows discriminating and identifying the different sources of dichroism.

For this purpose, the measurement of the Mueller matrix elements is best suited. The Mueller matrix is a 4 × 4 matrix that provides the most complete description of the optical response of the layers [11]. In general, the off diagonal elements m_{12}, m_{21}, m_{13}, and m_{31} are related with the linear dichroism, m_{14}, and m_{41} with the circular dichroism, m_{24}, m_{34}, m_{42}, and m_{43} with the linear birefringence and m_{23}, and m_{32} with the circular birefringence. In particular, the elements m_{12}, and m_{13} are, by definition, proportional to the difference of the transmitted intensity for light linearly polarized along the (100) and (010) axis, and (110) and (1-10) axis (linear dichroism), respectively, while m_{14} is proportional to the difference of the transmitted intensity for left and right circularly polarized light (circular dichroism) [12]. In a similar way, the same applies for differences in phase for the transmitted light for the corresponding birefringent elements.

With this in mind, in this work we present a methodology based on the Mueller matrix formalism that allows discriminating the different contributions to the global dichroic signal of artificial magneto-chiral structures. Our protocol is experimentally carried out by first studying pure Au split ring/ring structures [13] with chirality induced by an additional Au nanodisk at either edge of the split ring. This nanodisk breaks at the same time the in plane symmetry and contributes as an additional source of CD via optical anisotropy. This protocol is corroborated and contrasted with isostructural magneto-chiral entities, where the Au nanodisk is substituted by an Au/Co multilayer nanodisk with MO activity.

2. Fabrication of the structures

To achieve the mentioned structures, our approach will be to assemble the magneto-chiral system from individual plasmonic and MO building blocks, each of them responsible for different roles in the global properties of the system (see Fig. 1(a)). This way, an Au split ring will be used to generate a resonant system with a hot spot localized in the gap. An Au full ring will be attached to the split ring to shift the main resonances to the visible making them accessible to our experimental setups [14]. Then an Au or Au/Co multilayer nanodisk will be placed at either edge of the split ring, breaking the symmetry and giving rise to a chiral configuration (Fig. 1(b)). To experimentally realize such structures, we make use of multiaxial evaporation through hole masks, a technique with broad applications for the generation of 3D complex plasmonic and magneto-plasmonic structures [15-17]. In brief, a number or materials are evaporated onto a substrate mounted on a multiaxial holder. The presence on the surface of the substrate of a mask with nanoholes defined with standard hole mask colloidal lithography process [18] makes it possible to obtain systems with a variety of morphologies, from single disks, rods, split rings, rings, etc.

The typical dimensions of the obtained structures are: outer diameter of the nanoring structure around 290nm, disk height around 80nm, ring height around 20nm, gap height around 10nm, and central angle for the gap around 60 degree. A SEM image of a representative structure is shown in Fig. 1(c). The multilayer nature of the Au/Co disk with specific thicknesses of the Au and Co individual layers (typically 2.5 and 1.5 nm respectively) is selected to induce magnetic anisotropy perpendicular to the Au/Co interfaces, reducing largely the required magnetic field to saturate the structure along this direction [19]. Besides, this perpendicular magnetic anisotropy is an indication of the good quality of the Au/Co interfaces [20]. For these specific Au and Co thicknesses, interface anisotropy along the

Optics EXPRESS

surface normal overcomes shape anisotropy (which tends to orient magnetization in the field plane), resulting in a net out-of-plane magnetic easy axis, in contrast for example with a single Co layer embedded between two Au layers (Fig. 1(d)). This implies that only a small

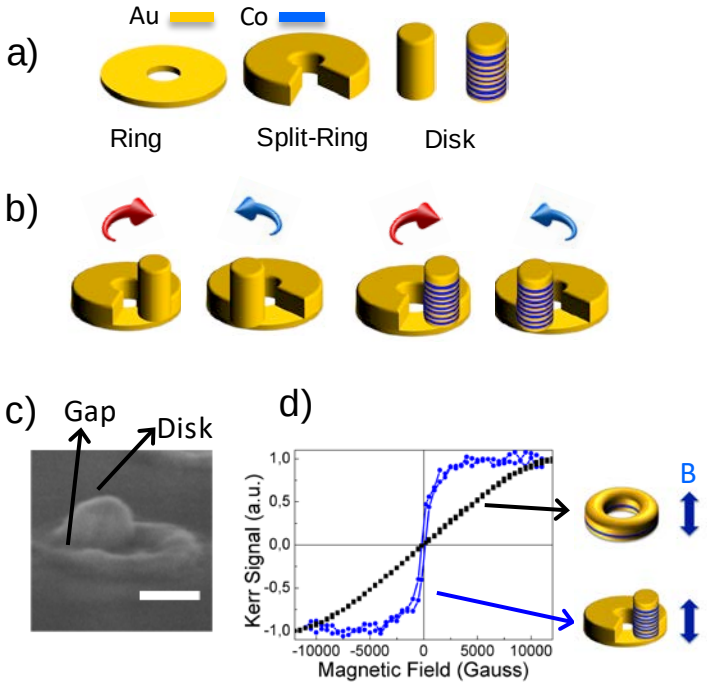

Fig. 1. (a) The different building blocks that will form part of the final structures. (b) Resulted chiral plasmonic and magnetoplasmonic metastructures fabricated and studied in this work. The specific location of the Au or Au/Co multilayer disk at either side of the split ring edge induces an in plane optical anisotropy and determines the handedness of the system. (c) SEM image of a representative structure obtained in this way. Scale bar: 100nm. (d) Comparative MO hysteresis loops for an Au/Co/Au ring structure with in plane magnetic anisotropy and a split ring/ring structure with an Au/Co multilayer, with perpendicular magnetic anisotropy. As it can be seen, magnetic saturation along surface normal requires a much smaller magnetic field for the multilayer case.

magnetic coil, instead of a bulky electromagnet, is required to carry out the measurements with the magnetic field along the surface normal, which is very convenient from the technical point of view, both for the experiments presented in this work as well as for its potential implementation as a sensing platform.

3. Preliminary symmetry considerations

Let's first consider two pure Au chiral structures (left elements in Fig. 1(b)), nominally identical apart from fabrication deviations, but with opposite chirality. In Fig. 2 we present relevant Mueller matrix elements and their relation with transmission intensities in forward and backward illumination.

As it can be seen, according to the definition of the shown elements and the specific illumination configuration, the measurement of m_{12} in forward m^F_{12} vs backward m^B_{12} illumination does not alter the result, since the relative position of the nanodisk along the x direction is not modified, and that along the y direction only changes sign, not modifying the resulting intensity along this direction. However, reversing illumination direction for the m_{13} element implies that the disk element will move from the y' to the x' direction resulting in a change in the sign of this element. Finally, if only chirality was present in the structure, the same value should be obtained for the m_{14} element measured in forward vs. backward

Optics EXPRESS

illumination, since the helicity of the structure does not depend on the illumination direction. However, the presence of an additional in-plane optical anisotropy induced by the in-plane

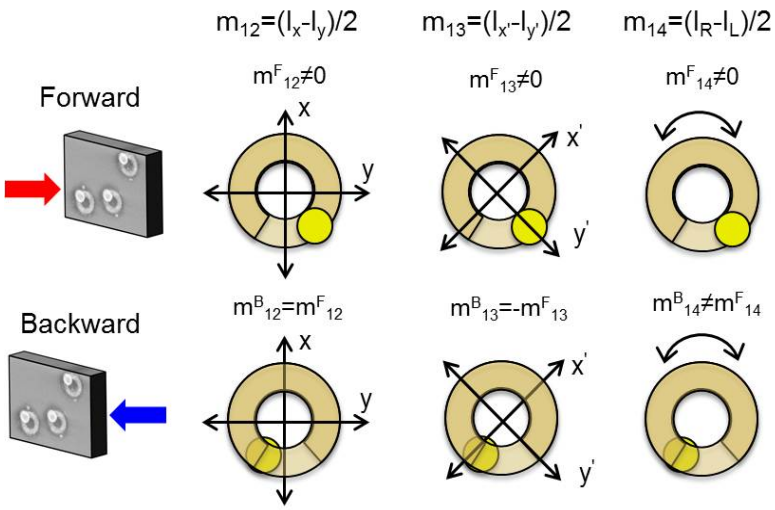

Fig. 2. Sketch of the measurement configurations and the Mueller matrix elements dependence on the specific light polarization relative to the structure main axes.

symmetry breaking of the nanodisk makes this situation change. Since the sign of the optical anisotropy contribution to m_{14} depends on the illumination direction, it will add up to the effect of the chirality along one illumination direction, but will be opposite along the other direction, obtaining different results for m_{14} in forward and backward illuminations (rightmost column in Fig. 2).

A quantification of the relative contributions to the measured magnitudes can be obtained formulating the Mueller matrix elements in terms of the Jones matrix elements of the nanoparticle layer. In particular, for forward illumination, m^F_{12}, m^F_{13}, m^F_{14}, and for backward illumination, m^B_{12}, m^B_{13}, m^B_{14}, can be written as:

$$\begin{aligned}
m^F_{12} &= (\frac{1}{2})(t_{xx}t^*_{xx} - t_{yy}t^*_{yy} - 4\,\mathrm{Re}(t_a t^*_{sy})) \\
m^F_{13} &= \mathrm{Re}((t_{xx}+t_{yy})t^*_{sy}) + \mathrm{Re}((t_{xx}-t_{yy})t^*_a) \\
m^F_{14} &= \mathrm{Im}((t_{xx}-t_{yy})t^*_{sy}) + \mathrm{Im}(((t_{xx}+t_{yy})t^*_a) \\
m^B_{12} &= (\frac{1}{2})(t_{xx}t^*_{xx} - t_{yy}t^*_{yy} + 4\,\mathrm{Re}(t_a t^*_{sy})) \\
m^B_{13} &= -\mathrm{Re}((t_{xx}+t_{yy})t^*_{sy}) + \mathrm{Re}((t_{xx}-t_{yy})t^*_a) \\
m^B_{14} &= -\mathrm{Im}((t_{xx}-t_{yy})t^*_{sy}) + \mathrm{Im}(((t_{xx}+t_{yy})t^*_a)
\end{aligned} \tag{1}$$

where t_{xx}, t_{yy}, t_{sy}, t_a, are the elements of the Jones matrix of the layer, which for the two illumination conditions can be written, using the elements for forward illumination, as [10]:

$$F:\begin{pmatrix} t_{xx} & t_{sy}+t_a \\ t_{sy}-t_a & t_{yy} \end{pmatrix}; B:\begin{pmatrix} t_{xx} & -t_{sy}+t_a \\ -t_{sy}-t_a & t_{yy} \end{pmatrix} \tag{2}$$

Formulating the non-diagonal elements in terms of their symmetric ($t_{sy} = (t_{xy} + t_{yx})/2$) and antisymmetric components ($t_a = (t_{xy} - t_{yx})/2$), allows discriminating the different contributions to the optical properties of the layer: t_{sy} depends on the optical anisotropy (in particular, on non-diagonal element, ε_{xy}, of the effective dielectric tensor of the layer); whereas t_a depends

Optics EXPRESS

not only on the intrinsic chirality, but also of the MO response of the active element. In this way, Eq. (1) are decomposed in terms of the contributions due to the optical anisotropy (t_{sy}) and due to chirality and/or MO activity (t_a). On the other hand, t_{sy} and t_a are smaller than t_{xx} and t_{yy} and, as discussed above, we should expect a similar value for m_{12} in forward and backward illumination. On the contrary, Eq. (1) also show that m_{13} and m_{14} may have contributions from both optical anisotropy and chirality. For example, the pure chiral contribution to the CD signal (or m_{14} element) is Im(($t_{xx} + t_{yy}$)t_a*), which can be obtained from $m_{14}^{Ch} = (m_{14}^{F} + m_{14}^{B})/2$, whereas, the optical anisotropy contribution is Im((t_{xx}-t_{yy})t_{sy}*), which can be obtained from $m_{14}^{Ansy} = (m_{14}^{F} - m_{14}^{B})/2$. This can be similarly applied for m_{13}.

4. Results: Au chiral structures

To experimentally test these arguments, in Fig. 3 we present representative Mueller matrix elements in forward and backward orientations for the fabricated pure Au chiral structures (left elements in Fig. 1(b)) with opposite handedness. The red and blue open dots correspond to forward and backward illumination measurements, respectively, and the samples are oriented with the line that connects the centre of the structure with the gap centre parallel to the vertical direction, as shown in Fig. 2. As it can be observed, elements m_{12}, m_{21}, m_{34}, related with the horizontal linear dichroism and birefringence, are very similar for both samples and do not change if the illumination direction changes. On the other hand, m_{13}, m_{31} and m_{24} elements, related to the ± 45° linear dichroism and birefringence, are also very similar for both samples, but change their sign when the illumination direction changes. Finally the elements m_{23}, m_{32} and m_{14}, related with both of the CD and circular birefringence (CB), have a very different spectral dependence when changing the illumination direction. This confirms the symmetry arguments discussed in Fig. 2: these last elements have contributions of both the chirooptical and in-plane optical anisotropy of the system and the different behaviours of these contributions respect to the change of illumination direction are responsible for the differences observed in the CD and CB signals (while chirooptical and anisotropic contributions add in one illumination direction, they subtract in the other).

These results clearly show that the fabricated structures have both in-plane optical anisotropy and chiral properties and make it therefore necessary to separate both contributions from the global dichroic response of the system. To do this, we first assume that the layer system can be viewed as an effective medium, in which case the electromagnetic fields in the layer can be related by the following constitutive relations [21,22]:

$$\begin{bmatrix} \vec{D} \\ \vec{B} \end{bmatrix} = \begin{bmatrix} \varepsilon_0 \varepsilon_{eff} & i\kappa_{eff}/c \\ -i\kappa_{eff}/c & \mu_0 \mu_{eff} \end{bmatrix} \begin{bmatrix} \vec{E} \\ \vec{H} \end{bmatrix} \tag{3}$$

where ,ε_{eff}, μ_{eff} and κ_{eff} are the effective dielectric, permeability and magneto-electric (chiral) tensors of the layer, respectively. In the visible range the permeability is 1, and for normal incidence only the ε_{xx}, ε_{yy}, and ε_{xy} elements of the dielectric tensor and κ_{xx}, and κ_{yy} of the chiral tensor (in particular κ_{xx} + κ_{yy}) play a major role in the propagation of the electromagnetic fields. Within this approach, it is already possible to separate the different electromagnetic functionalities of these structures, say purely optical and chiro-optical contributions. The obtained diagonal/off-diagonal elements of the dielectric and chiral tensor respectively are shown in Fig. 4.

Optics EXPRESS

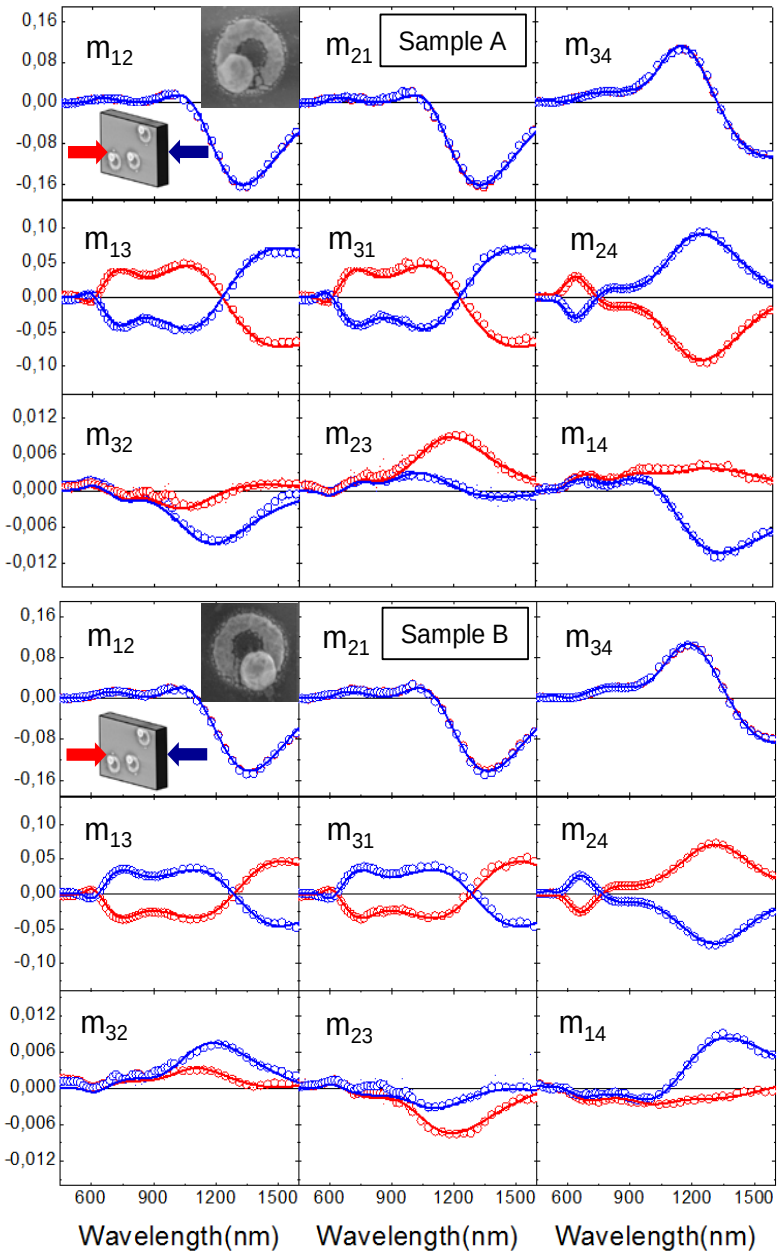

Fig. 3. Representative Mueller matrix elements (normalized to m_{11}) of the two pure Au chiral samples of Fig. 2 for forward (red) and backward (blue) illuminations. The dots are experimental data and the lines theoretical simulations.

If we first take a look at the diagonal elements of the effective dielectric tensor, ε_{xx} and ε_{yy} (left column in Fig. 4), they are very similar for both samples, with two resonances polarized along the x axis, located at around 600 nm and 1300 nm, respectively, and two resonances polarized along the y axis and located at around 600 nm and 1100 nm, respectively. On the other hand, the non-diagonal element of the effective dielectric tensor, ε_{xy} (central column in Fig. 4), show two main features located at around 600 nm and 1300 nm. The intensity and shape of this non-diagonal element are very similar for both samples, but the signs are

Optics EXPRESS

opposite, since the optical anisotropies due to the presence of the additional Au dot at either side of the split ring gap have opposite signs. Finally, regarding the elements of the chiral tensor (right column in Fig. 4), $K = (\kappa_{xx} + \kappa_{yy})/2$, they also show two main features located in the same spectral range than ε_{xy} and, since the two structures have opposite chirality, their corresponding elements of the chiral tensor also have opposite signs.

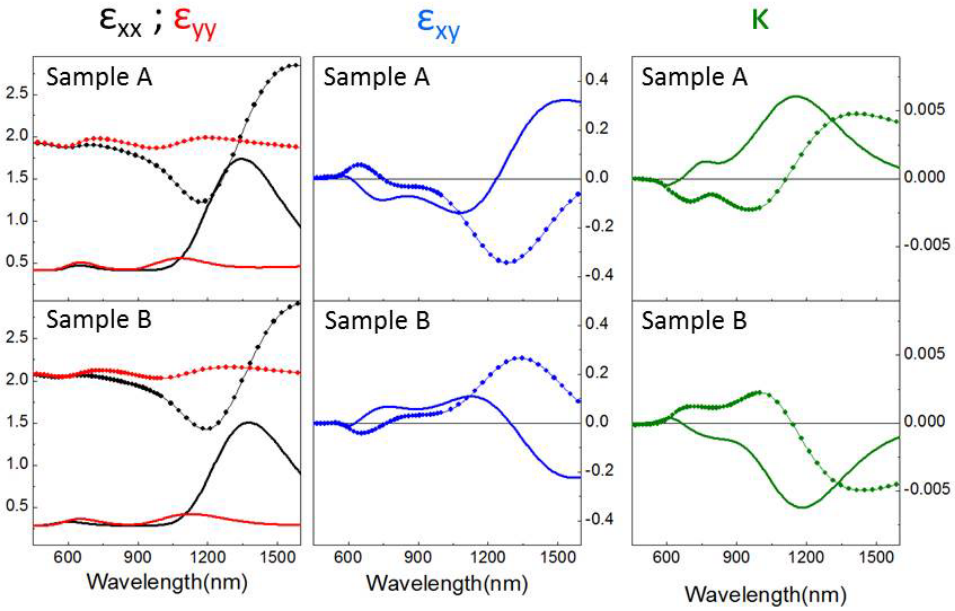

Fig. 4. Effective dielectric and chiral tensors of the pure Au chiral nanoparticle layers of sample A and B (Fig. 3) as a function of the wavelength. The curves with full dots correspond to the real part of the different elements of the dielectric and chiral tensors. The full line curves correspond to the imaginary part of the different elements of the dielectric and chiral tensors.

Just for consistency, with these obtained dielectric and chiral tensor elements, the Mueller matrix elements of the structure can be conversely calculated, (full curves in Fig. 3) finding a very good agreement with the experiments for different considered in-plane orientations of the sample with respect to the light polarization.

A very convenient figure of merit normally used to characterize the chirooptical properties of a system is the anisotropy factor g, defined as [23]:

$$g = 2\frac{A^+ - A^-}{A^+ + A^-}; A^{+,-} = \log(T^{+,-}) \tag{4}$$

where $A^{+,-}$ is the absorption for left-handed (-) and right–handed (+) circularly polarized light, respectively, which can be related to the normalized value of m_{14} as follows:

$$g = \frac{\log(\frac{1+m_{14}}{1-m_{14}})}{\log(T(1-m_{14}^2)}; T = \frac{T^+ + T^-}{2} \tag{5}$$

Both magnitudes, g and m_{14}, are therefore closely related and can be both used to characterize the dichroic nature of the structure. In Fig. 5 we present the spectral dependence of g due exclusively to the pure chiral contribution obtained substituting in Eq. (5) m_{14} by m_{14}^{Ch}. As it can be observed this g spectrum of sample A is nearly the mirror image of the g spectrum of sample B. This compares very reasonably with g values obtained for other structures of similar nature and under similar measurement configurations [24-26].

Optics EXPRESS

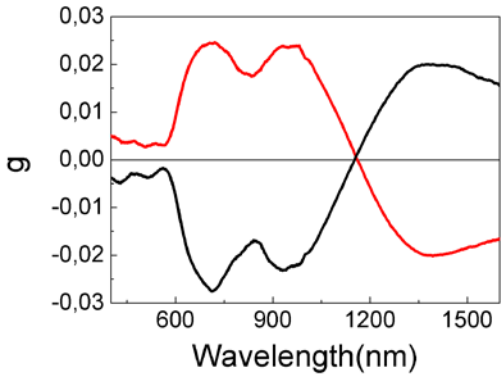

Fig. 5. *g* spectra of pure Au chiral samples A and B.

Therefore, being aware of the different contributions to the global CD of our system and making adequate use of the Mueller matrix formalism in forward and backward illumination, it is possible to separate them and get a quantitative determination of the true chirality via the *g* parameter. For completeness, we would like to point out that the different contributions to the global CD could also be obtained from both m_{14} and m_{41} parameters, but, to obtain these two parameters, requires a more complex experimental set-up than a simple CD transmission spectrometer.

5. Results: Au/Co multilayer disk–Au chiral structures

Once our complete methodology is presented and applied to a chiral plasmonic system with no MO component, we turn now to apply it to an equivalent system where the Au disk that endorses the chiral character is substituted by a MO Au/Co multilatyer disk (two right panels in Fig. 1(b)). As mentioned in previous paragraphs, the contribution to the CD from the MO part (MCD) will have similar symmetry properties than the chiral contribution, both maintaining sign upon illumination direction reversal. In addition, this identical symmetry property makes the MO functionality an ideal modulation mechanism for the pure chirooptical activity in any illumination configuration.

Two types of magneto-chiral structures were fabricated, each of them consisting of two samples with opposite chiralities, with different design parameters to obtain different spectral responses and make it possible to explore the considered magnetic modulation in different situations.

The whole same procedure to extract *g* presented in the previous section for pure Au chiral structures can be applied to these MO-chiral structures. In Fig. 6 we present the spectral dependence of *g*, already without any optical anisotropy contribution. Due to the presence of the MO component, two spectra for each structure are presented, corresponding to magnetic saturations of this component along opposite directions by the application of a high enough magnetic field (0.3 – 0.4T). Therefore, the corresponding MCD signal of the MO component will add or subtract to the pure chiral component, leading to the results presented in Fig. 6.

The red curves correspond to the sample with one chirality and the black curves to the sample of opposite chirality. Focusing our attention to the structure shown on the left, the spectra have two main features located around 750 nm and around 1150nm, respectively. As expected, the spectra of the two samples with opposite chirality are nearly mirror like images of one another. On the other hand, for each sample, the difference in the *g* value for positive and negative magnetic fields is similar for both samples, regardless of the sign of the chirality, reaching a maximum of around 25% at 740 nm. Interestingly enough, this magnetic modulation is obviously much higher for the high energy feature than that of the low energy one. This may be due to the different spatial localization of the electromagnetic (EM) field in

Optics EXPRESS

the region of the MO nanodisk for both resonances, even though both of them present large chirooptical activity. The sign contribution of the chirooptical and MO components is also confirmed in these spectra: perfect mirror spectra are obtained for samples with opposite chiralities and also opposite magnetic fields, so that both chirality and MO effects contribute in the same direction to the total value of *g*. On the other hand, a clear change in the spectral dependence and electromagnetic field localization can be obtained by changing the morphological parameters of the structure, as shown in the right panel of Fig. 6. Modes at different energies are excited in this case, with maximum g at around 800 nm. In this case, however, the magnetic modulation of *g* is much smaller, probably due to a weaker localization of the EM field in the MO component, and as a consequence to a smaller modulation effect. Theoretical calculations to determine the actual EM field distributions in the different cases would support this assumption, but are out of the aim of this work.

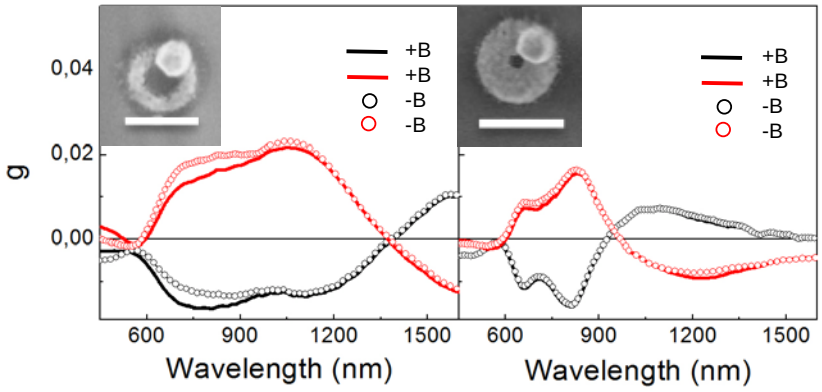

Fig. 6. Spectral dependence of *g* for the Au/Co multilayer disk-Au chiral structures. The optical anisotropy contribution has been removed with the methodology introduced previously. Black and red curves represent the spectral responses for the two structures with opposite chirality. Solid curves are for + B magnetization and dotted curves for –B magnetization. Scale bar: 300nm.

Going back to the structure shown in the left panel of Fig. 6, it is a clear example of potential platform for magnetic modulation of chirooptical effects for the detection of chiral species. The relatively small magnetic fields needed to saturate these structures and the spectral tunability of the MO active feature (in this case the high energy one), suggests that it could be used as transducer for a magnetic modulation concept. AC measurements in which the chiral signal can be controlled by an external oscillating magnetic field would improve the signal to noise ratio in the sensing platform and therefore the detection limits established for equivalent, non magnetically modulated, structures. Besides, the MO activity of magneto-plasmonic nanoparticles is proportional to the EM field inside the ferromagnetic component of the nanoparticle [13,27]. Therefore, the magnetic modulation of the chiro-optical properties offers a simple way to probe the EM distribution of the chiral resonances and the regions of the nanoparticle where the adsorption of molecules should produce a higher impact on the chirooptical response. Detailed design of these platforms to spectrally position the magnetically modulated feature in the adequate wavelengths matching those of characteristic transitions of chiral molecules would allow for an optimization of this concept. In addition, the multi-layered nature of the MO element, with the Co layers embedded in Au, is a warrantee for its chemical stability against eventual chemical agents present in the sensing process.

Finally, the use of plasmonic resonances has also been theoretically proposed to increase the so-called magneto chiral effect [28,29]. This effect manifests as intensity changes in unpolarized light transmitted through chiral ferromagnetic entities upon magnetization or

Optics EXPRESS

helicity reversal [30], recently observed in nanoscale chiral nanomagnets [31]. The corresponding asymmetry factors obtained in these cases reach values of the order of 10^{-4} T^{-1}.

6. Conclusions

We have applied an experimental methodology to separate the different sources of CD originated from complex chiro-optical and magneto-chiral structures. For this purpose the Mueller matrix formalism in forward and backward illumination has been utilized. The different illumination direction dependence of the sign of the dichroic signals due to optical anisotropy and chiral configuration has been exploited to differentiate them. Additionally, magneto-chiral systems of similar spatial configuration have been fabricated and studied, quantifying the pure chiral magnitude g and its magnetic field modulation. Magnetic modulations of g of around 25% at around 740 nm have been obtained.

Funding

We acknowledge financial support from MINECO through project AMES (MAT 2014-58860- P). H. Y. Feng thanks the funding from CSC (Chinese Scholarship Council), Grant No. 201206220112.